EUROPEAN ORGANIZATION FOR NUCLEAR RESEARCH
CERN - ACCELERATORS AND TECHNOLOGY SECTOR

CERN/ATS 2010-003

STATIC HEAT LOADS IN THE LHC ARC CRYOSTATS: FINAL ASSESSMENT

C. Maglioni, V. Parma

Abstract

This note presents the final assessment of the static heat loads in the LHC arc cryostats, using different experimental methods during the first commissioning period in 2007. This assessment further develops and completes previous estimates made during the commissioning of sector 7-8 [1]. The estimate of the helium inventory, a prerequisite for the heat load calculation, is also presented.

Heat loads to the cold mass are evaluated from the internal energy balance during natural as well as powered warm-ups of the helium baths in different subsector. The helium inventory is calculated from the internal energy balance during powered warm-ups and matched with previous assessments. Furthermore, heat loads to the thermal shield are estimated from the non-isothermal cooling of the supercritical helium in line *E*.

The comparison of measured heat loads with previous estimates and with budgeted values is then presented, while their correlation with some important parameters like insulation vacuum pressure and some heat interception temperatures is proposed and discussed.

CERN-ATS-2010-003
22/01/2010

Geneva, Switzerland

January 2010

1. INTRODUCTION

During the development phase of the LHC cryostats, systematic laboratory heat load measurements were performed to validate the design and completed by first thermal performance assessments of the main prototype components. From these tests a reference heat load budget was established and used to size the cryogenic plant and distribution system. The resulting budgeted static loads, including the contribution from QRL valves, amount to 0.195 W/m at the temperature of 1.9 K, 0.14 W/m at an average design temperature of 7.5 K and 4.5 W/m at an average design temperature of 57.5 K [2].

The thermal performance of the LHC arc cryostat was then validated in 2003 on the 107 m-long prototype (String 2, [3] and [4]), which comprised two Short Straight Sections (SSS) and six dipoles. Measurements of the total helium vaporization rate gave a first estimate of a total heat load at 1.9 K of 21.2 ± 1.9 W, i.e. 0.20 ± 0.02 W/m, close to the budgeted values, but on which the influence from the string extremities (DFB and return boxes) and of additional instrumentation could not be estimated with precision.

The first commissioning of LHC, between January 2007 and July 2008, provided an excellent possibility to confirm this performance directly on the installed machine.

This work presents the assessment and validation of static heat loads to the 1.9K cold mass and to the 50-65 K thermal shield, carried out during this commissioning period. Results are then compared with budgets and discussed, while a sensibility analysis on the influence of different important parameters like insulation vacuum pressure and cryogenic line temperatures is proposed.

2. MATERIALS AND METHODS

2.1. Machine layout

Each of the 8 LHC sectors comprises 154 dipoles and about 54 SSS housing the main quadrupoles, operating in a pressurized 1.9 K static helium bath, enclosed in a common and continuous cryostat [5]. A cryogenic distribution line (QRL) alongside the continuous magnet cryostat provides the distribution of helium to magnets and cryostats via transverse piping (jumpers).

The cold masses containing the superconducting magnets are cooled via a separate cryogenic circuit, featuring an internal bayonet heat exchanger (HET) operating at low-pressure saturated helium II (16 mbar), in which liquid is fed from the cryogenic line *C* through the Joule-Thompson valve and vapours are pumped via the cryogenic line *B* back to the cryogenic plant [6]. This cooling loop extends over a total length of 107 m, covering 2 quadrupoles and 6 dipoles, and ends in a helium phase separator for collection of liquid in excess and where a level gauge is housed (Figure 1). The common pressurized 1.9 K static helium bath of the cold masses, a so-called *cryogenic subsector*, extends over the length of 2 cooling loops (214 m) and is delimited by plugs[1].

[1] Hydraulic plugs are placed inside standard interconnections and can be considered as leak-tight. "Hydraulic restrictions" are used instead in all the other interconnections within the subsector, which allow a certain amount of helium flow. This is important for what later discussed in Paragraph 7.1.

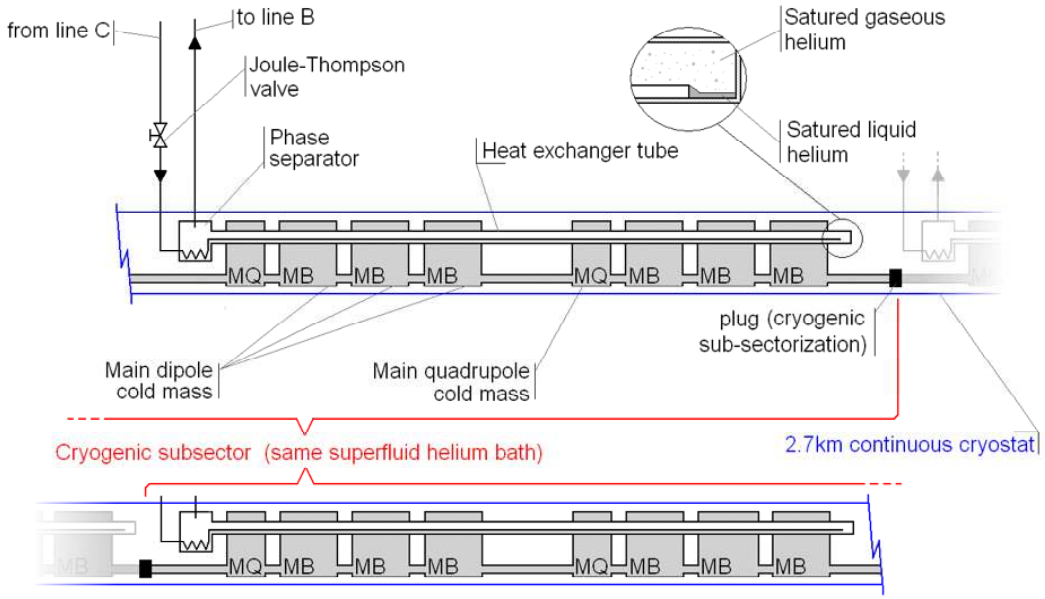

Figure 1. Schematic layout of a cryogenic subsector (two standard arc cells).

The insulation vacuum (nominal pressure $\leq 10^{-6}$ mbar) of the 2.7 km-long continuous cryostats is also sectorized by vacuum barriers at every cryogenic subsector. The cold masses are thermally insulated by multilayer insulation (MLI) blankets inside their cryostats, which are also equipped with a thermal shield with MLI, actively cooled at 50-65 K by supercritical helium flowing in line *E* continuously along the full length of a sector. The same line is also used as heat intercept for the magnet supports. An additional heat interception for the supports and for other components is provided by line *C'*, cooled at a nominal temperature range of 5-10 K (Figure 2).

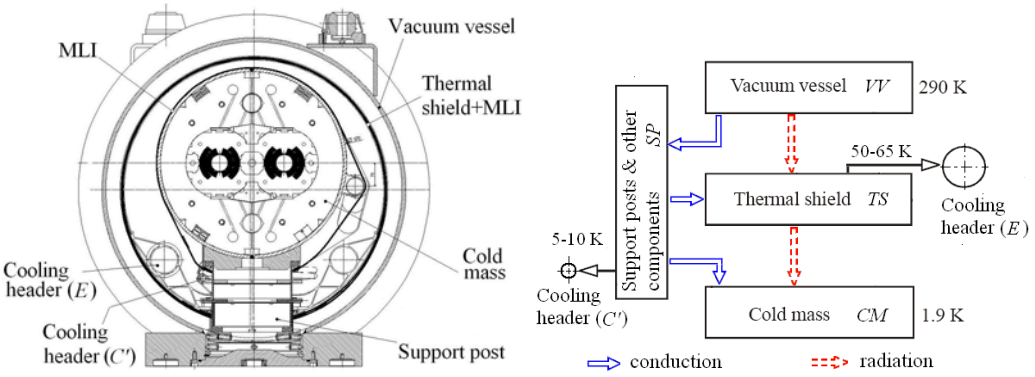

Figure 2. Cross section of a dipole cryostat and schematic of heat flows and heat intercept temperatures.

2.2. Thermal shield static heat load

The thermal shield receives heat mainly by radiation from the vacuum vessel and by conduction through different heat intercepts (support posts mainly but also dipole corrector current feed-throughs (DCF), beam tubes pumping manifolds, etc), as schematically shown in Figure 2. In stationary conditions, the heat intercepted by the

thermal shield is given by the enthalpy change during the non-isothermal heating of gaseous helium along line *E*. For each cryogenic subsector, assuming it's uniformly distributed, the heat load to the thermal shield per unit length is:

$$W_E = \frac{\Delta H_S}{L_S} = \frac{\left(\dot{m}_E \cdot \Delta h_S\right)}{L_S} \tag{1}$$

where $\Delta h_S = \Delta h_S(p,T)$ (J/kg) is the specific mass enthalpy change along the L_S-long segment of line *E* corresponding to the considered subsector (m), while $\dot{m}_E$ is the helium mass flow evaluated from the overall measured pressure drop Δp along line *E* (kg/s) [1]. Using the data acquired during the LHC operation runs, the resulting heat load per unit length is calculated with (1) at every data acquisition time-step and then averaged over a long time period, in order to avoid the influence of data acquisition frequency and to minimize uncertainties[2].

The specific enthalpy balance $\Delta h_S = h_{i+1}(T_{i+1}\,,\, p_{i+1}) - h_i(T_i\,,\, p_i)$ between the two sensors *i* and *i+1* is numerically evaluated with HePAK [7], using temperature and pressure readings, and assuming stationary conditions. But since only two pressure sensors are available within the sector and since the low value of the overall pressure drop has limited influence on the enthalpy, pressure was assumed constant along the whole line *E* for enthalpy calculation purposes ($p_i = p_{i+1}$).

Estimating the helium enthalpy balance inside the thermal shield cooling line results in a net load, which is the difference between the heat received by the shield and the heat leaving to the cold mass (Figure 2):

$$W_E = W_{VV \to TS} - W_{TS \to CM} \tag{2}$$

Hereafter, when referring to *thermal shield heat loads*, the meaning is therefore *net static heat load adsorbed by header E*.

2.3. Cold mass static heat load assessment methods

For what stated in Annex 7.1, each cryogenic subsector has to be separately considered and no further subdivision should be made referring to the helium bath. Hence, hereafter all quantities refers to overall subsector quantities and all variables are average subsector variables.

As long as it remains a closed system in respect to the rest of the machine, the total power adsorbed by the helium bath within the subsector can be estimated as the change of its internal energy over time. Precisely, when supply of sub-cooled helium to the heat exchanger is stopped, the helium bath within the subsector cold mass starts a natural warm-up (phase *A*, Figure 3) that is due, in static conditions, to the heat

[2] Data were taken from Timber-SCADA interface, during a period of three days with one minute frequency. SCADA is the Supervisory Control And Data Acquisition system. The chosen period lasted from 18:00 of 6th to 18:00 of 9th, April 2007. The acquisition was made in scale down repeat mode. The period chosen was the most representative compromise between nominal and stable equilibrium conditions for the thermal shield. Moreover both cold masses and line *C'* were in nominal and stable conditions during this period. Supply temperature of header *E* (T_{supply}) was stable since a few days, with variations of less than 4% around the mean value, and also during the entire chosen period. Its value, however, was lower than nominal (44.6 ± 0.8K instead of 50K).

received from the thermal shield and from various heat intercepts (see also Figure 2) and represents the *natural* static heat load per unit length to the cold mass:

$$W_{CM} = \frac{\Delta U_{CM}^{A}}{\Delta t^{A} \cdot L_S} = \frac{\sum_i m_i \cdot \Delta u_i^{A}}{\Delta t^{A} \cdot L_S} \qquad \text{(phase } A\text{)} \qquad (3)$$

where L_S is the subsector length (m), $u = u(p,T)$ is the specific internal energy as a function of temperature and pressure readings, while m_i and $\Delta u_i{}^{A}$ are respectively the mass content (kg) and the variation of specific internal energy (J/kg) of the cold mass i-th component [3] during the phase A, lasting Δt^{A} (s).

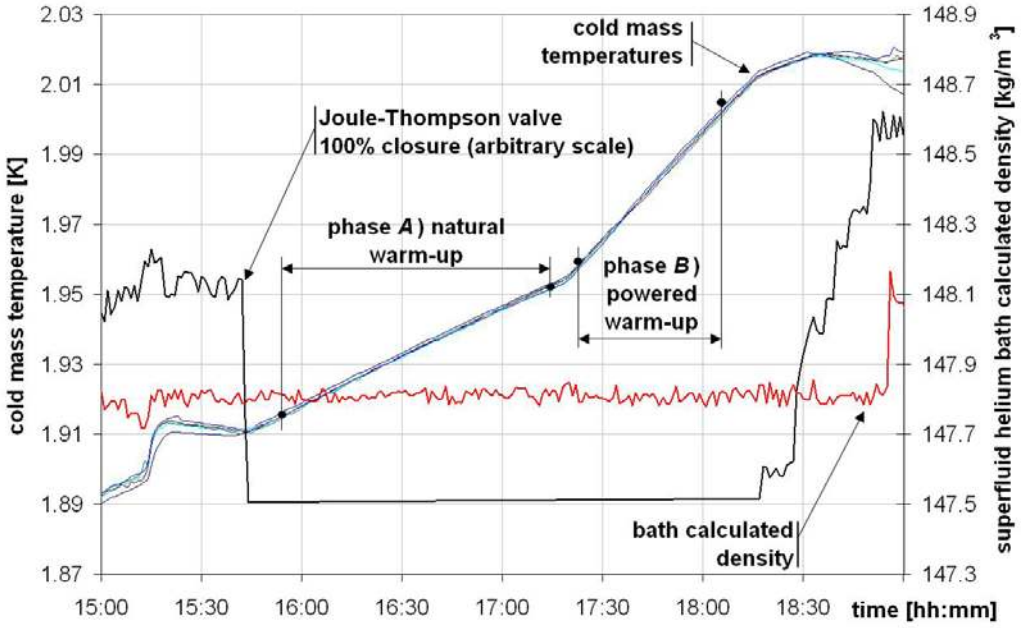

Figure 3. Temperature evolution, calculated helium density (in red) and feeding valve opening (in black) in one subsector during a test.

After some time, a faster warm-up is forced by injecting a known electrical power (typically 40 W per subsector) in the cold mass bath via built-in heaters, giving a second trend in the temperature increase (phase *B*). The total incoming heat now results from the sum of the previous *natural* load and the injected power:

$$W_{CM} + W_{IN} = \frac{\Delta U_{CM}^{B}}{\Delta t^{B} \cdot L_S} = \frac{\sum_i m_i \cdot \Delta u_i^{B}}{\Delta t^{B} \cdot L_S} \qquad \text{(phase } B\text{)} \qquad (4)$$

The first heat load calculating method (method I) consists in considering both warm-ups sequentially (phases *A* and *B*) and solving the system of equations (3, 4) which yields the two unknowns, namely helium content m_{He} and cold mass heat load per unit length W_{CM}:

[3] See Annex 7.2.

$$m_{He} = \frac{L_S \cdot W_{IN} + \left(\frac{\Delta U^A_{Cu}}{\Delta t^A} - \frac{\Delta U^B_{Cu}}{\Delta t^B}\right) + \left(\frac{\Delta U^A_{StSt}}{\Delta t^A} - \frac{\Delta U^B_{StSt}}{\Delta t^B}\right)}{\left(\frac{\Delta u^B_{He}}{\Delta t^B} - \frac{\Delta u^A_{He}}{\Delta t^A}\right)} \approx \frac{L_S \cdot W_{IN}}{\left(\frac{\Delta u^B_{He}}{\Delta t^B} - \frac{\Delta u^A_{He}}{\Delta t^A}\right)} \quad (5)$$

$$W_{CM} = \frac{m_{He} \cdot \Delta u^A_{He} + \Delta U^A_{StSt} + \Delta U^A_{Cu}}{\Delta t^A \cdot L_S} \approx \frac{m_{He} \cdot \Delta u^A_{He}}{\Delta t^A \cdot L_S} \quad (6)$$

Once the average helium content $\overline{m}_{He}$ is determined, based on different tests in different subsectors, natural warm-ups were sufficient to measure static heat loads elsewhere in other cryogenic subsectors whenever they occurred[4] during the LHC commissioning, using directly equation (3) (method II, phase *A* only).

Measurements were made acquiring data every minute during periods of one to a few hours on a number of subsectors. Insulation vacuum pressure and temperatures of lines *C'* and *E* were also monitored in order to assess their influence on heat loads.

3. RESULTS AND DISCUSSION

3.1. Thermal shield static heat load

Regarding the thermal shield performance, only one test was carried out in one sector in stable condition with temperature of line *E* between 45 K and 55 K (5 to 10 K lower than nominal). The resulting heat load along the sector varies between 3.07 W/m and 4.27 W/m, in average 18% lower than budgeted.

Since temperature of line *E* was lower than nominal, these estimates are to be considered as upper limits. Results are graphically shown in Figure 4, where the computed heat load profile is compared to the expected one and also the temperature profile of line E along the sector is shown.

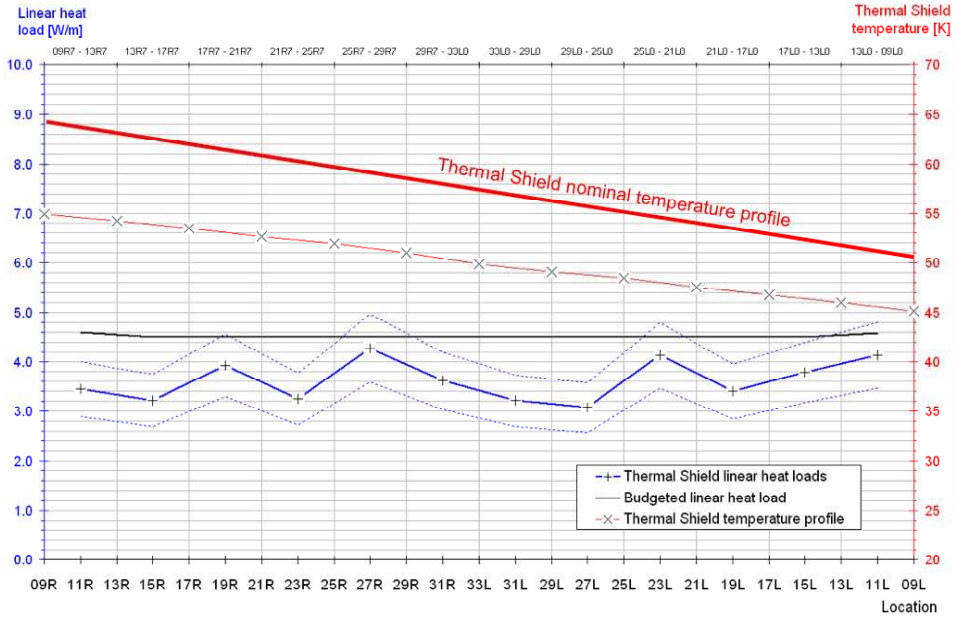

Figure 4. Thermal shield static heat load profile along the sector (sector 7_8)

[4] Not all the occurred temperature drifts were exploitable, since some necessary conditions had to be respected during the tests for the calculation to be validated (see Annex 7.3).

The heat load calculation includes three standard deviations for random errors where the mean heat load W_E is averaged over a sample of 4320 values (one minute acquisition frequency over a period of three days).

It should be kept in mind that the heat load profile is obtained from the enthalpy balance of the coolant, which had a supply temperature lower than the nominal design value. Indeed, the value of T_{supply} does not only affect the overall temperature profile along the cooling line, as said, but also strongly determines the enthalpy levels of heat exchange along the whole line. Increasing T_{supply} from the actual to the nominal value, say from 44.6K to 50K, and considering the reasonable hypothesis that ΔT between two generic sensors would however remain the same, the enthalpy balance $\Delta h = \Delta h(\Delta T, T_{supply}, p)$ would slightly decrease. Hence the heat load affecting the thermal shield would decrease further below the calculated profile in full nominal conditions.

3.2. Cold mass static heat load

Table 1 presents test results from the applications of the two methods to different subsectors together with parameters to which heat loads are correlated, namely temperatures of the lines *E* and *C'* and insulation vacuum pressure. The analysis presented hereafter assumes no sector-specific dependence of the results. Results are also presented graphically in Figure 5, where tests 9 and 10 are detailed for each individual subsector.

Table 1. Test results for the heat loads to the cold mass.

Test #	Test method	Cryogenic subsector_ machine sector	Cold mass heat load [mW/m]	Properties within the subsector		
				Line *E* [K]	line *C'* [K]	Insulation Vacuum [mbar]
1	I	15-17_R7	**130.4 ± 32.9**	52.2 ± 5	10 ± 1	$0.9 \cdot 10^{-7}$
2	I	23-25_R7	**126.5 ± 32.5**	50.5 ± 5	10 ± 1	$0.9 \cdot 10^{-7}$
3	I	27-29_R7	**126.0 ± 31.8**	49.6 ± 5	10 ± 1	$4.2 \cdot 10^{-7}$
4	II	15-13_L3	**206.8 ± 34.1**	51.5 ± 5	20 ± 1 [a]	$4.3 \cdot 10^{-7}$
5	II	11-13_R2	**184.9 ± 32.4**	43.5 ± 5	20 ± 1 [a]	$5 \cdot 10^{-7}$
6	I	19-17_L6	**133.1± 35.1**	43.5 ± 5	7 ± 1	$5.3 \cdot 10^{-7}$
7 [b]	I	11-13_R5	**141.3 ± 25.4**	53 ± 5	5.5 ± 1	$3.9 \cdot 10^{-7}$
8	II	31_R7-33_L8	**271.6 ± 31.5**	50 ± 5	6 ÷ 8 ± 1(unstable)	$1 \cdot 10^{-5} \div 1 \cdot 10^{-4}$ [c]
9	II	Average on sector 7_8	**147.7 ± 36.5**	42.5 ÷ 53 ± 5	6 ± 1 (unstable)	$2.4 \cdot 10^{-7}$ (average)
10	II	Average on sector 5_6	**152.3 ± 31.5**	46 ÷ 54 ± 5	6 ± 1 (unstable)	$2.5 \cdot 10^{-7}$ (average)

[a] Line *C'* not cooled during the test.
[b] Magnet quench occurred in this subsector a few hours earlier, possibly increasing heat loads.
[c] Degraded vacuum due to leaks, slightly variable value.

From tests 1, 2, 3, 6 and 7, the average helium content has been calculated to be 26.8 ± 3.1 l/m, to be compared with the previously estimated value of 25.12 ± 0.47 l/m [8]. This estimate is increased of +6.7%, which falls within the helium content error band of ±11.6%.

What it is clearly visible from all tests except 4, 5, 7 and 8 (discussed hereafter) is that heat loads are roughly 30% lower than the budget estimate of 195 mW/m. This can be in part explained by the lower than nominal temperature in line *E*, a common feature for all these tests, thus reducing conduction heat through the support posts and radiation heat from the thermal shield to the cold mass. Also, insulation vacuum

pressure were slightly lower than maximum nominal pressure ($1 \cdot 10^{-4}$ Pa), which can aid the heat load reduction.

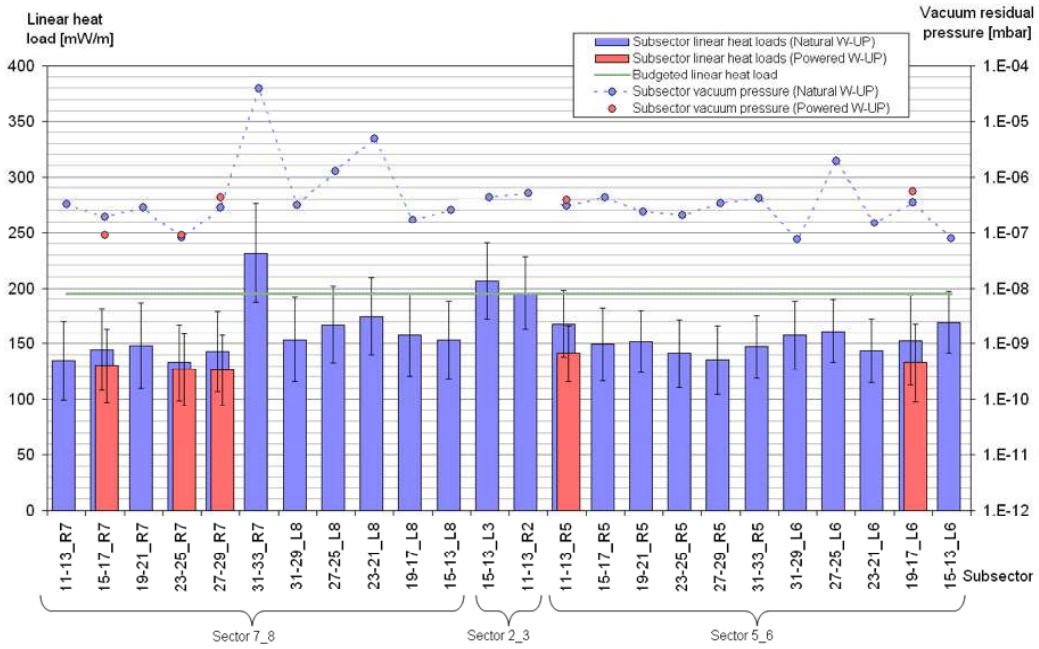

Figure 5. All calculated subsector heat loads per unit length. Natural warm-up (method II) in light blue, powered warm-up (method I) in light red. In green is plotted the budget estimate, while with points and dotted line is represented the insulation vacuum pressure profile (logarithmic scale).

However test 7, which has the closest to nominal temperatures in lines E and C', yields a heat load which remains ~27% lower than nominal. Similar values result from the average over whole sectors 7_8 and 5_6 (tests 9 and 10), which leave the margin of ~24% and ~22% from budgeted value respectively.

A clearer correlation between temperature of line *E* and heat load to the 1.9K helium bath is seen by comparing tests 6 and 7, where an increase of 9.5 K, while keeping all other variables fixed, translates into an increase in heat load of 6% (12% when also line *C'* is off-nominal, comparing tests 5 and 4).

The major influence to the heat load is nevertheless led by line *C'* operating temperature: when this line is not cooled (tests 4 and 5), an increase in heat loads up to 39% is observed (comparing tests 5 and 6, Figure 6). This large effect results from different additional heat loads, since line *C'* intercepts heat from supports and also from other components. About one half of the additional heat load may be imputed to the cold mass support posts [9], while the additional heat through other components, like power leads feed-through and beam-screens supports, could explain the remaining contribution.

Finally test 8, in a subsector with degraded vacuum due to helium leaks, yields heat loads which are more than twice higher than those of test 2, where temperatures of the cryogenic lines are comparable. Considering all results, heat loads increase up to 61% when residual insulation pressure raises to the order of $1 \cdot 10^{-5} \div 1 \cdot 10^{-4}$ mbar, while an increase of ~22% is recorded when pressure drops to $1 \cdot 10^{-6} \div 1 \cdot 10^{-5}$ mbar and of ~14% when residual pressure is at the maximum nominal value of $1 \cdot 10^{-6}$ mbar (Figure 7).

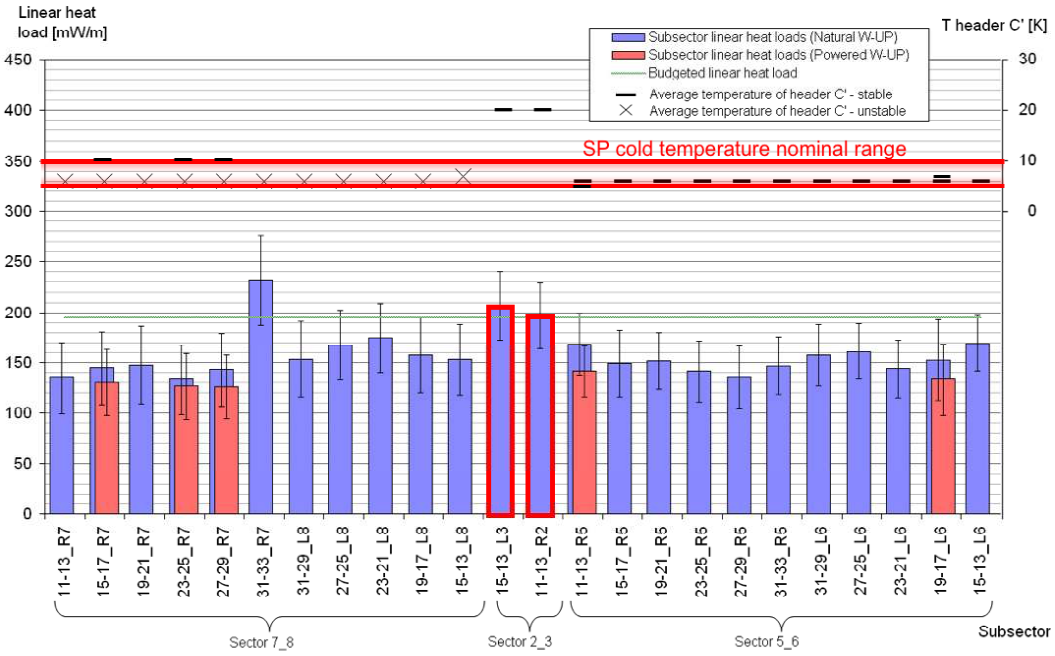

Figure 6. Correlation between heat loads and support post cold interception temperature (header C'). Presented statistical values are calculated on the basis of red bound-evidenced cases.

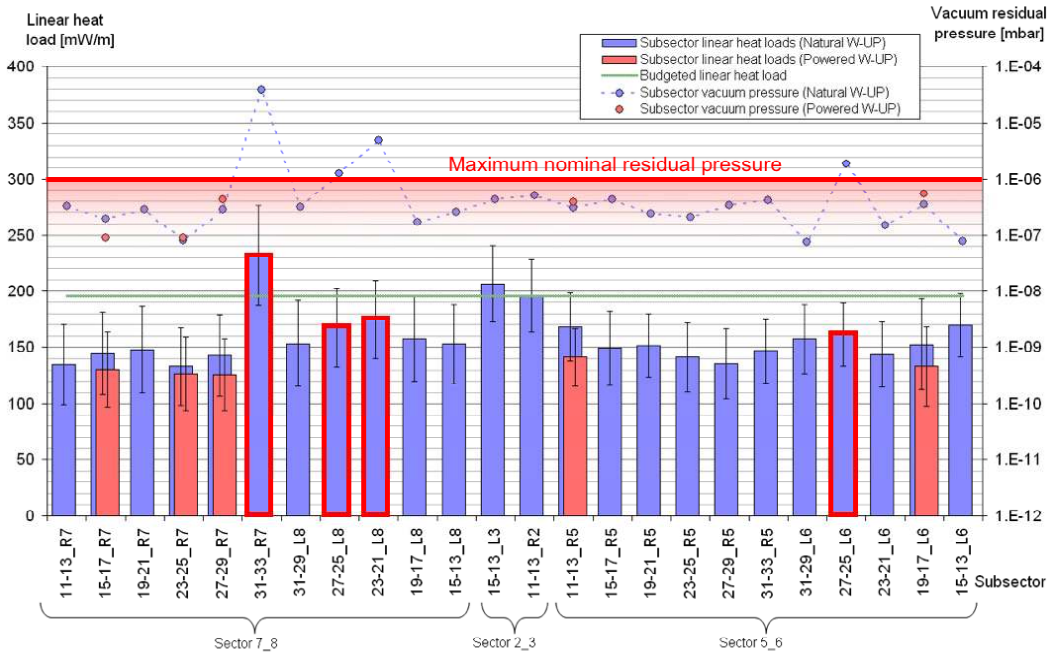

Figure 7. Correlation between heat loads and vacuum residual pressure. Presented statistical values are calculated on the basis of red bound-evidenced cases.

Extrapolating from the most representative value of 141.3 mW/m (test 7), to evaluate the heat load under perfectly nominal conditions, 14% is added due to nominal insulating pressure, and 3% due to nominal temperature of line *E*. This estimate leads to the value of 166 mW/m, which is still lower than budgeted value by ~ 15%, to be compared to an average heat load error band of 17.5%.

It should be noted, finally, that results from the method II are in average higher than those from method I, indicating an underlying effect that is not still understood and probably depends on measurement methods and conditions.

4. CONCLUSIONS

During hardware commissioning of the LHC, the assessment of static thermal heat loads of cryostats in different sectors was performed [10]. Even taking into account the uncertainties of the methods applied for thermal shield and cold mass heat loads, the thermal performance of the LHC arc-cryostats is well within budgeted values and measurement results made on the prototype String 2.

The method based on combined natural and forced temperature drifts below the lambda temperature of a complete and isolated cryogenic subsector yields the most trustworthy values. Heat loads at 1.9 K are about 27% lower than budgeted when operating the cryostat at temperatures close to nominal, 15% lower if the result is extrapolated from measurements made when temperature of the thermal shield was lower than nominal. The heat loads to the thermal shield, estimated on one sector only, are also considerably below nominal (-18%), and would further decrease operating it at its nominal temperature.

These results also validate the performance of the LHC magnet cryostats after long term (up to 3 years) outdoor storage prior to installation [11] and shows that installation and interconnection activities have not degraded in any significant way the thermal performance of the cryostats.

Finally, the average helium content of standard arc cryomagnets has been calculated as a result of these analyses and fits well with previous estimates.

5. ACKNOWLEDGEMENTS

We wish to thank the cryogenic operation team of TE-CRG for its collaboration and availability in running dedicated experiments that have made these heat loads measurements possible.

6. REFERENCES

[1] Maglioni, C. et al., *Assessment of Static Heat Loads in the LHC Arc, from the Commissioning of Sector 7-8*, LHC-Project-Note 409, CERN, Geneva 2007.

[2] Tavian, L. et al., *Heat Load Assessment*, http://lhc-mgt-hlwg.web.cern.ch/lhc-mgt-hlwg/, CERN, Geneva 2001.

[3] Bergot, J.B. et al., *Thermal Performance of the LHC Short Straight Section Cryostat*, LHC Project Report 571, CERN, Geneva 2002.

[4] Poncet, A. et al., *Final Design and Experimental Validation of the Thermal Performance of the LHC Lattice Cryostats*, Advances in Cryogenic Engineering – Vol 49A, 487-493, 2004.

[5] Brunet, J.C. et al., *Mechanical Design and Layout of the LHC Standard Half-Cell*, Proceedings of the 1997 Particle Accelerator Conference – Vol 3 (1997), 3368-3370.

[6] Lebrun, Ph., *Cryogenics for the Large Hadron Collider*, IEEE Transactions on Applied Superconductivity, ISSN 1051-8223, 2000.

[7] Cryodata Inc., *User's Guide to HEPAK Version 3.4*, Cryodata Inc, USA 1999.

[8] Maglioni, C. et al., *Assessment of Average Helium Quantity per Unit Length of LHC Arc Cold Masses*, LHC-Project-Note 408, CERN, Geneva 2007.
[9] Parma, V. et al. *Thermal Performance of the Supporting System for the Large Hadron Collider (LHC) Superconducting Magnets*, Advances in Cryogenic Engineering, Vol. 45A, 795-802, 2000.
[10] Serio, L. et al., *Validation and Performance of the LHC Cryogenic System Through Commissioning of the First Sector*, Adv. Cryo. Eng. 53B, 1411-1418.
[11] Seyvet, F. et al. *Long Term Stability of the LHC Superconducting Cryodipoles After Outdoor Storage*, IEEE Transactions on Applied Superconductivity, Vol. 16-2, 180-184, 2006.
[12] Van Sciver, S.W., *Helium Cryogenics*, ISBN 0-306-42335-9, 1986.

7. ANNEX

7.1. Calorimetric measurements sensitivity in superfluid helium

The calculation methods presented in this note are based on superfluid helium transformations and properties. In order to understand the sensitivity of measurements made and set limits on the validity of the heat load assessment, the heat transport capacity of superfluid helium in the practical case of study has to be evaluated. This property is theoretically described by equation:

$$\dot{q}^n = K_{SC}(p,T)\frac{dT}{dx} \tag{7}$$

where $n = 3$ in order to be able to use the software HePAK[5]. In equation (7) $\dot{q}$ is the steady-state heat flux conducted through superfluid helium in the longitudinal dimension (W/m^2) of a tubular conduit of length dx (m) with ends maintained with a temperature difference dT (K), while K_{SC} is helium superfluid thermal conductivity function (Figure 8).

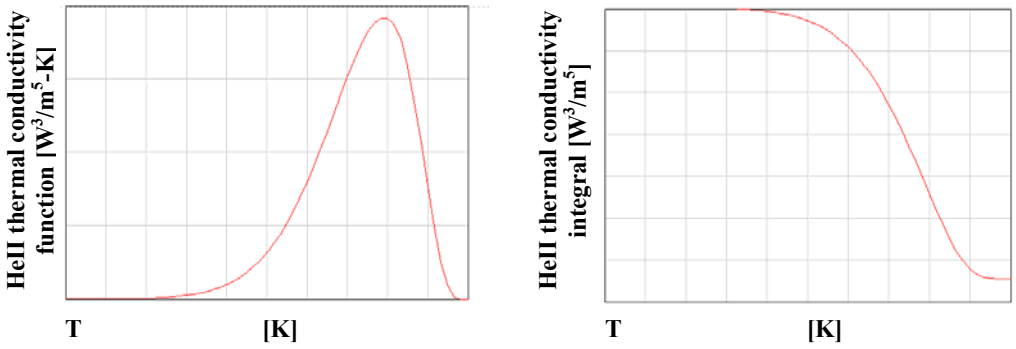

Figure 8. Superfluid thermal conductivity function (on the left) and its integral over temperature (on the right)

[5] Experimentally, this exponent has been shown to vary from below 3 to nearly 4 and, theoretically, it should be equal to 3, which is the value that fit HePAK data. Some Authors use the best-fit value of 3.4, but in any case the agreement between data and correlation remains acceptable [12].

Considering the simplifying configuration of two adjacent dipoles at the uniform temperatures of 1.9 K and 1.9+δ K respectively, the temperature gradient is concentrated within their interconnection and integration of equation (7) leads to

$$\dot{q}^3 L = 4\left[KI\left(\overline{p},T_C\right) - KI\left(\overline{p},T_W\right)\right] \tag{8}$$

where L represents the interconnection length (m), T_C = 1.9 K and T_W = 1.9+δ K. The function KI is the integral over temperature (at constant pressure p equal to its average value $\overline{p}$) of the superfluid thermal conductivity function (Figure 8).

$$KI = \int_{T_C}^{T_W} K_{SC}\left(\overline{p},T\right) dT \tag{9}$$

In this configuration the heat flow transport between the two dipoles is driven by the helium free cross-section within the interconnection (9.5E-3 m^2). Assuming also the hypothesis of constant helium mass flow all along the cooling bayonet[6], some further simplification can be made and the energy balance of the system (two adjacent dipoles plus their interconnection) leads to the result plotted (in blue) in Figure 9.

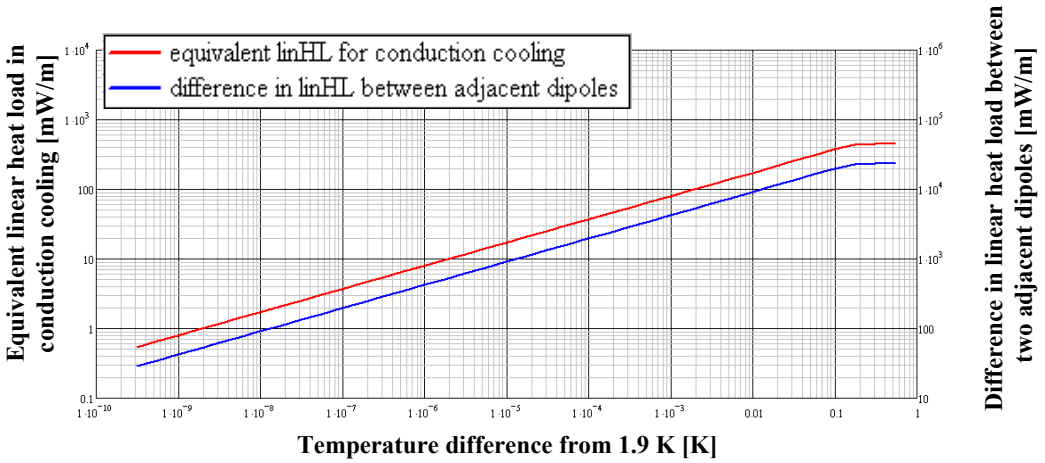

Figure 9. Correlation between heat transport properties of superfluid helium and measurement sensitivity in LHC practical cases.

To obtain a temperature difference δ = 0.001 K between two adjacent dipoles, which represents the order of magnitude of a minimum readable variation in thermometer measurements on cold masses, a difference in their respective linear heat loads of at least 4 W/m is necessary (right-hand axis): hence, apart from extremely bad situations, no heat load inconsistency may ever be found between different dipoles within the same subsector[7], and any non-uniformity has not to be considered as real but as a result of sensor calibration, data acquisition and data manipulation. In other words, the thermometer accuracy (1E-3 K) does not allows to distinguish heat load variations within a subsector, but only between different subsectors where the

[6] This assumption simplifies the calculation and gives rise to a very small error in the result (~ +0.1%).
[7] Applied in a practical case, the value of 4 W/ m would be an extremely bad situation since it has to be compared to the budgeted value of 0.195 W/m. Calculation does not take into account any eventual interruption or higher-than-expected impedance in the interconnections.

helium free cross-section in the interconnection becomes extremely small due to the presence of a leak-tight hydraulic plug.

Another interesting case is when the bayonet ceases to work, so that the relative cryogenic cell turns out to be cooled exclusively by conduction through superfluid helium by the adjacent cell within the same subsector. In this case too, the heat flow is solely constrained by superfluid helium free cross-section within the interconnection between the two cells.

Assuming a uniform temperature of 1.9 K for the well cooled cell and a uniform distributed budgeted heat load over the whole subsector, equation (8) is still valid using L for the cell length (106.9m) and T_C = 1.9K. In this case T_W represents the warmest reached temperature, at distance L from the interface between the two cells.

The result is also plotted in fig, in red: a uniform heat load of 0.2W/m over the non-cooled cell (left-hand axis) leads to a maximum temperature difference $\Delta T_{max} \sim$ 0.01K (horizontal axis), a value which is in good agreement with observations. The resulting heat flux through the cell is of the order of 0.2 W/cm^2 and T_{max} = 1.91 K. This case allows to later considering the contribution to cell cooling by conduction through adjacent cell.

7.2. Heat capacities at constant density

The heat capacity to be taken into account to calculate the internal energy variation in a standard LHC arc cryomagnet is provided by the cold mass constituting materials and by the superfluid helium content of the bath: with an average estimated value of 25.12 ± 0.47 liter/m [8], the heat capacity of helium in superfluid state is highly dominant (98.3%), which allows considering only its heat capacity, together with the contribution of copper (0.01%) and steel.

These three different contributions are highlighted in Figure 10 in function of cold mass temperature for an isochoric transformation[8]. As it can be seen considering the case of a dipole, the error made using the approximated formulae (5) and (6), which only consider the helium contribution and neglect steel and copper ones, is negligible in the range of temperatures of superfluid helium.

7.3. Cold mass static heat load calculation: necessary conditions

Some necessary conditions had to be respected during the tests for the calculation to be validated[9]:

I. In order to make use of equations (3) and (4), the subsector must be a closed system, so that all the valves to the QRL have to be closed and leak tight during the warm-up. This assumption can be verified post-mortem by checking that helium in the cold mass bath undergone an isochoric transformation (red curve in Figure 3**)**.

[8] In the real case this kind of transformation is not possible for the whole range of temperature shown in the graph, since valves would open before He II transforms into He I.

[9] During the first LHC commissioning, there have been some natural warm-ups due to different issues, but only few of them presented the optimal conditions required for the assessment. Where these conditions were not perfectly respected, some corrections applied.

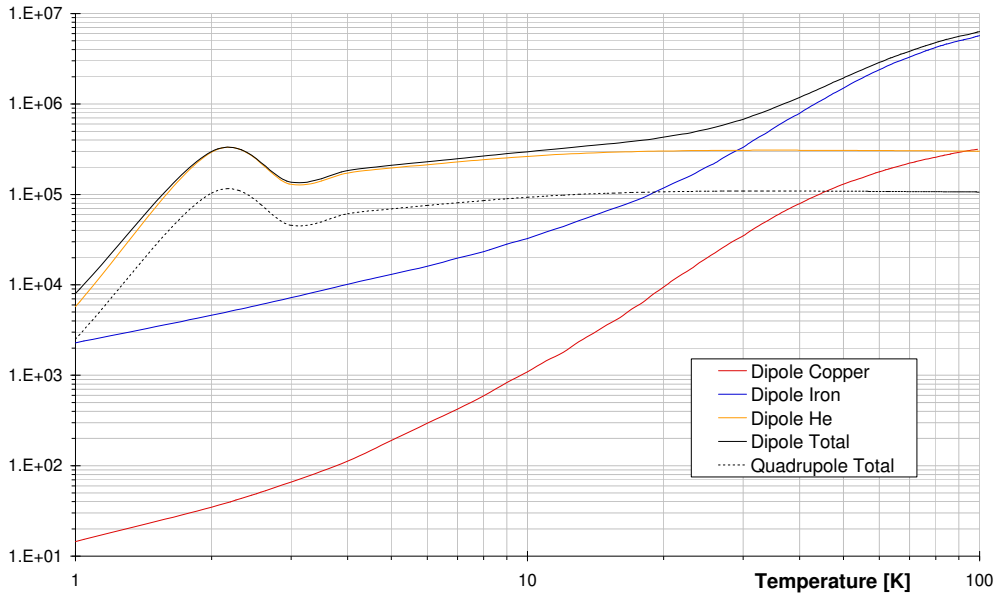

Figure 10. Dipole and quadrupole cryomagnet heat capacities in function of temperature at constant density (ρ = 147 kg/m^3)

II. In equation (3), the internal energy $u = u(p,T)$ is derived from point measurements of temperature and pressure (one temperature sensor every cold mass, one pressure sensor every subsector). Uniform temperature is required all along the cold mass and during the whole warm-up to obtain a correct assessment, a condition that can be assured only for temperatures below T_λ, taking advantage of the very high heat transport capacity of pressurized helium in superfluid state. Hence, any test has to necessarily end well before helium reached the normal state, that is:

$$T \in [T_i,\ T_\lambda[\approx [1.9\text{K},\ 2.15\text{K}] \tag{10}$$

III. Within the defined temperature range (10), only the linear part of temperature drift has to be considered, neglecting thermal inertia (non-linearity at the end of the drift) and liquid helium discharge from the bayonet to the phase separator (non linearity at the beginning of the drift).

IV. As soon as the feeding of sub-cooled helium stops, if pumping in returning line *B* is also stopped vapors starts to condensate within the bayonet. This condensation produces a release of additional heat to the cold mass, which superposes to the previous one, reflecting in a increase of helium level in the phase separator:

$$W_{CM}^{+} = \dot{m}_{vap} \cdot \frac{LH}{L_S} = \frac{\Delta V_{L,ref} \cdot \rho_L}{\Delta t_{ref}} \cdot \frac{LH}{L_S} \tag{11}$$

where LH is helium latent heat (J/kg) and m_{vap} is the vapors mass flow (kg/s), which can be estimated proportionally to the helium level increase as the variation in time of a reference volume $\Delta V_{L,ref} / \Delta t_{ref}$ (m^3/s) of liquid helium (density ρ_L, kg/m^3). If this is the case during tests, the additional load has to be

taken into account throughout equation (11), or a period of at least twenty-thirty minutes has to be left after the supply had stop and before the data acquisition starts. On the other hand, if pumping in returning line *B* is kept active, the vapors are quickly evacuated and no additional load is found.

V. Cold mass conditions should be kept stable since some time before starting any test, with temperature as low as possible: this assures stable and uniform conditions within the superfluid helium bath, leaving enough room in the temperature range for the test to be performed.